Synthesis, Photophysics, Electrochemistry, and Electrogenerated Chemiluminescence of a Homologous Set of BODIPY−Appended Bipyridine Derivatives

ARTICLE *in* THE JOURNAL OF PHYSICAL CHEMISTRY C · SEPTEMBER 2011

Impact Factor: 4.77 · DOI: 10.1021/jp204487r · Source: PubMed

Published in final edited form as:
J Phys Chem C Nanomater Interfaces. 2011 September 15; 115(36): 17993–18001. doi:10.1021/jp204487r.

Synthesis, Photophysics, Electrochemistry and Electrogenerated Chemiluminescence of a Homologous Set of BODIPY-Appended Bipyridine Derivatives

Joel Rosenthal, **Alexander B. Nepomnyashchii**, **Julia Kozhukh**, **Allen J. Bard**, and **Stephen J. Lippard**
Department of Chemistry, Massachusetts Institute of Technology, Cambridge, MA 02139-4307 and Department of Chemistry and Biochemistry, The University of Texas at Austin, Austin, Texas 78712

Abstract

Two new 2,2′-bipyridine (bpy) based ligands with ancillary BODIPY chromophores attached at the 4 and 4′-positions were prepared and characterized, which vary in the substitution pattern about the BODIPY periphery by either excluding (**BB1**) or including (**BB2**) a β-alkyl substituent. Both absorb strongly throughout the visible region and are strongly emissive. The basic photophysics and electrochemical properties of **BB1** and **BB2** are comparable to those of the BODIPY monomers on which they are based. The solid-state structures and electronic structure calculations both indicate that there is negligible electronic communication between the BODIPY moieties and the intervening bpy spacers. Electrogenerated chemiluminescence spectra of the two Bpy-BODIPY derivatives are similar to their recorded fluorescence profiles and are strongly influenced by substituents on the BODIPY chromophores. These 2,2′-bipyridine derivatives represent a new set of ligands that should find utility in applications including light-harvesting, photocatalysis, and molecular electronics.

Keywords

BODIPY; bipyridine; electrochemistry; photophysics; electrogenerated chemiluminescence

Introduction

Polypyridyl-based ligands are ubiquitous in coordination chemistry and polypyridine complexes of transition metals have a long[1] and rich history.[2] In particular, 2,2′-bipyridine derivatives can form complexes with many different metals, especially those having d^3, d^6, d^8 or d^{10} electron configurations.[3] The ability of bipyridine to act as a strong σ-donating chelate coupled with its π–acidic nature allows the polypyridyl unit to stabilize transition metals in a wide range of oxidation states and gives rise to complexes that exhibit a plethora of interesting photophysical and redox properties.[3,4] Metal complexes supported by bipyridyl ligands have therefore been the subject of many studies dealing with catalysis, molecular electronics, and photochemistry.[5] The chromophoric nature of these species has led to bipyridyl derivatives being used in optoelectronic devices aimed at light harvesting and energy storage.[4,6,7] For example, the most efficient dye sensitized solar cells (DSSCs) described to date are generally based upon ruthenium polypyridyl complexes,[8–10] and platinum bipyridyls are good photosensitizers for charge separation[11] and hydrogen

Supporting Information. Tables of computational coordinates; tables of X-ray crystallographic data including fully labeled thermal ellipsoid plots, and tabulated bonding metrics. This material is available free of charge via the Internet at http://pubs.acs.org.

generation from water.[12–14] In both these cases, the polypyridyl complex is responsible for light absorption via formation of MLCT excited states and either electron or energy transfer. Although the excited states of such complexes have appropriate redox properties to drive charge separation and energy storage, the extinction coefficients are relatively modest ($\varepsilon \approx 10^3 - 10^4$ M^{-1} cm^{-1}) and are significantly lower than those displayed by more strongly absorbing organic chromophores such as porphyrinoids[3,15,16] and laser dyes.[17,18]

Strongly absorbing organic sensitizers have been used for energy harvesting applications[19,20] but often suffer from accelerated degradation and photobleaching as compared to metal polypyridyls. One attractive solution to this issue is the development of hybrid systems, which take advantage of the excellent stability and redox properties of metal polypyridyl complexes and the large absorption cross sections exhibited by organic chromophores. 2,2′-Bipyridine derivatives containing conjugated thiophenes,[21] triphenyl amine,[22] or carbazole[23] antennae have previously been incorporated into DSSCs. Although these systems display greater spectral breadth, in many cases, extinction coefficients are still in the range of $\varepsilon = 10^4$ M^{-1} cm^{-1}. In an attempt to improve the ability of such assemblies to harvest light, we developed a set of 2,2′-bipyridine derivatives containing intensely absorbing laser dyes at the 4- and 4′-positions. In designing these new ligands, we employed boron-dipyrromethane (BODIPY) dyes, which offer strong absorption and emission properties in the visible region coupled with high photostability.[24,25] Furthermore, similar systems have been shown to be able to serve as a light harvesting antennae for platinum bipyridine based photosensitizers.[26]

In synthesizing a set of ligands in which the BODIPY chromophores are linked directly to the ligand, we are in a position to determine how the intervening 2,2′-bipyridine spacer influences the excited state and redox properties of this construct. Basic photophysical, electrochemical, and electrogenerated chemiluminescence (ECL) studies of the 2,2′-bipyridine–BODIPY (bpy-BODIPY) has illluminated the nature of the interaction between the BODIPY dyes and the influence of the conjugated linker on the stability of the radical ions produced upon reduction and oxidation. ECL studies along with cyclic voltammetric (CV) experiments indicate that the major photophysical properties associated with previously studied BODIPY monomers[27–33] are maintained in the bpy-BODIPY systems and that the substitution pattern about the BODIPY periphery greatly impacts these properties.

Experimental Section

Materials

Silica gel 60 (70 – 230 and 230 – 400 mesh, Merck) and Merck 60 F254 silica gel (pre-coated sheets, 0.2 mm thick) were used for column and analytical thin-layer chromatography, respectively. Solvents for synthesis were of reagent grade or better and were dried by passage through activated alumina then stored over 4 Å molecular sieves prior to use.[34]

Physical measurements

^{1}H NMR spectra were recorded at 25 °C in the MIT Department of Chemistry Instrumentation Facility (DCIF) on a Varian 300 or 500 MHz spectrometer, referencing to the residual proton resonance of the deuterated solvent. All chemical shifts are reported using the standard δ notation in parts-per-million; positive chemical shifts are to higher frequency from the given reference. Low-resolution mass spectra were obtained with an Agilent 1100 Series LC/MSD mass spectrometer and high resolution mass spectral analyses were performed in the MIT DCIF. UV/vis absorption spectra were acquired on a Cary 50 spectrometer using screw cap quartz cuvettes (7q) from Starna. Acquisitions were made at

25.0 ± 0.05 °C. Fluorescence spectra were obtained on a Photon Technology International (PTI) fluorimeter at 25.0 ± 0.5 °C following previously described procedures.[35]

Electrochemistry and Electrogenerated Chemiluminescence

Electro-chemistry experiments were carried out using a three-electrode setup with a 0.0314 cm^2 platinum disk working electrode, a platinum auxiliary electrode, and a silver wire quasireference electrode. A straight working electrode (disk oriented horizontally downward) was used for the CV measurements and a J-shaped electrode (disk oriented vertically) was used for the ECL experiments. Working electrodes were polished prior to every experiment with 0.3 μm alumina particles dispersed in water, followed by sonication in ethanol and water for several minutes. All glassware was oven dried for one hour at 120 °C prior to transferring into an Ar filled drybox. All solutions were prepared inside the drybox and sealed in a conventional electrochemical apparatus with e metal rods for electrode connections. Cyclic voltammetry and chronoamperometry experiments were carried out with a CHI instruments model 660 electrochemical workstation. The supporting electrolyte used for electrochemistry experiments was 0.1 M *n*-tetrabutylammonium hexafluorophosphate ($TBAPF_6$) and ferrocene was used to calibrate the Ag wire quasireference electrode (QRE) taking the Fc/Fc^+ potential as 0.342 V vs SCE.[36] Chronoamperometry and scan rate CV experiments were used to determine the diffusion coefficients of the dyes. ECL spectra were generated by using benzoyl peroxide as a coreactant and spectra obtained by stepping to 80 mV from reduction peaks at a pulse frequency of 1 Hz or with a step time of 1 min. Spectra were recorded with a Princeton instruments Spec 10 CCD camera (Trenton, NJ) with an Acton SpectPro-150 monochromator cooled with liquid nitrogen to −100 °C. ECL-CV simultaneous experiments were done prior to spectral measurements to assure the presence of ECL emission. In this case a multichannel Eco Chemie Autolab PGSTAT100 (Utrecht, The Netherlands) was used for collection of the signal and a photomultiplier tube (Hamamatsu R4220, Tokyo, Japan) was used as a detector. Voltage for the PMT, −750 V, was provided by a Kepco power supply (New York, NY) and the signal from the PMT to the potentiostat was transferred through a multimeter (Keithley, Solon, OH). Digital simulations were done using Digisim computer software (Bioanalytical Systems, West Lafayette, IN).[37–40]

X-ray Crystallography

X-ray diffraction experiments were performed on single crystals grown by the slow evaporation of chloroform solutions of **BB1** and chloroform/acetonitrile solutions of **BB2**, respectively. Crystals were removed from the supernatant liquid and transferred onto a microscope slide coated with Paratone N oil. Crystals were mounted in Paratone N oil at the end of a cryoloop and frozen at 110 K under a cold nitrogen stream controlled by a KRYO-FLEX low-temperature apparatus. Data collection was performed on a Bruker APEX CCD X-ray diffractometer with graphite-monochromated Mo-K_α radiation (λ = 0.71073 Å) controlled by the *SMART* software package,[41] and were refined using *SAINT* software.[42] Empirical absorption correction was performed with *SADABS*.[43] The structure was solved by direct methods and refined by full-matrix least-squares on F^2 using the *SHELXTL-97* software package.[44] Possible higher symmetries were evaluated by *PLATON*.[45] Non-hydrogen atoms were located and their positions refined anisotropically. Hydrogen atoms were assigned idealized positions and given thermal parameters either 1.2 (non-methyl hydrogen atoms) or 1.5 (methyl hydrogen atoms) times the thermal parameters of the atoms to which they are attached.

Computations

Geometry optimizations, frequency calculations, and molecular orbital calculations were performed in Gaussian 03[46] using the B3LYP/6-311G(d) basis set. Crystallographic coordinates were used as starting points for geometry optimizations, and only positive frequencies were found for the optimized structures. Molecular orbitals were visualized with the VMD software.[47] All calculations were performed in the gas phase.

[2,2′-Bipyridine]-4,4′-dicarboxylic acid (1)

Selenium dioxide (4.0 g, 36 mmol) was added to a solution of 1.5 g (7.2 mmol) of 4,4-dimethyl-2,2′-bipyridine in 100 mL of dioxane. The reaction mixture was heated at reflux while stirring vigorously for 3.5 h. After cooling to room temperature the mixture was filtered to remove all solid materials and the solvent was removed from the filtrate to deliver a red solid. Recrystallization of this crude material from EtOH at −40 °C produced an off-white solid, which was subsequently dissolved in 25 mL of concentrated nitric acid. The acid solution was heated to reflux while stirring under air. This reaction was accompanied by the formation of red vapors within the reaction vessel. After 4 h the reaction mixture was cooled to 0 °C and 175 mL of ice-cold water was added to precipitate a light yellow solid. The solid was isolated by filtration and dried under vacuum to afford 0.77 g of the title compound (44%). ^{1}H NMR (300 MHz, $CDCl_3$, 25 °C), δ/ppm: 8.91 (d, 2H), 8.84 (s, 2H), 7.91 (d, 2H).

[2,2′-Bipyridine]-4,4′-dicarbonyl dichloride (2)[48]

[2,2′-Bipyridine]-4,4′-dicarboxylic acid (0.62 g, 2.5 mmol) was suspended in 40 mL of thionyl chloride. The reaction mixture was heated at reflux under nitrogen for 36 h. Over the course of the reaction the starting dicarboxylic acid slowly dissolved in the thionyl chloride. Following removal of the thionyl chloride under reduced pressure, the resultant yellow residue was dried in vacuo for 3 h. The product was used immediately for the subsequent reaction without further purification. The yield was assumed to be quantitative.

Bpy-BODIPY1 (BB1)

The [2,2′-bipyridine]-4,4′-dicarbonyl dichloride, assumed to be 2.5 mmol, prepared in the previous step was dissolved in 100 mL of chloroform and the resulting solution was sparged with nitrogen for 40 min. Following the addition of 2,4-dimethylpyrrole (1.0 mL, 10.15 mmol) to the degassed solution, the reaction was heated at 70 °C under nitrogen for 75 min. During the course of this reaction the solution gradually developed a dark red color. After removal of the solvent by rotary evaporation, the resulting dark residue was redissolved in 100 mL of toluene and chloroform (9:1). To the solution was added 5.0 mL of TEA and the solution was stirred under air for 30 min, after which time 6.5 mL of $BF_3{\cdot}OEt_2$ was added. The solution was stirred at 60 °C for 2 h and the solvent was once again removed by rotary evaporation. After redissolving the dark colored residue in DCM, the organic solution was washed with water three times and dried over Na_2SO_4. The crude product was purified on silica, eluting first with $CHCl_3$ and slowly increasing the polarity of the mobile phase to 5% MeOH in $CHCl_3$. The crude material thus obtained was purified further on a second column of basic alumina, eluting first with DCM and slowly moving to a mobile phase of 3% DCM in MeOH to deliver 340 mg of the desired product as a red powder (21%). ^{1}H NMR (300 MHz, $CDCl_3$, 25 °C), δ/ppm: 8.79 (d, 2H), 8.45 (s, 2H), 7.27 (d, 2H) 2.58 (s, 12H), 1.43 (s, 12H). HR-ESIMS $[M + H]^+$, m/z: Calcd for $C_{36}H_{35}B_2F_4N_6$, 649.3045. Found, 649.3074.

Bpy-BODIPY2 (BB2)

This compound was prepared in a manner identical to that described for **BB1** above by using 2,4-dimethyl-3-ethylpyrrole in place of 2,4-dimethylpyrrole. The title compound was

isolated in 23% yield. ^{1}H NMR (300 MHz, $CDCl_3$, 25 °C), δ/ppm: 8.76 (d, 2H), 8.50 (s, 2H), 7.33 (d, 2H), 2.53 (s, 12H), 2.28 (q, 8H), 1.36 (s, 12H), 0.97 (t, 12H). HR-ESIMS $[M + H]^+$, m/z: Calcd for $C_{44}H_{51}B_2F_4N_6$, 761.4297. Found, 761.4341.

Results and Discussion

Synthesis and Characterization

The synthetic strategy used to prepare the homologous bipyridine-BODIPY architectures bpy-BODIPY-1 (**BB1**) and bpy-BODPIY-2 (**BB2**) is presented in Scheme 1. The synthesis of the two homologues is similar, with the derivatives **BB1** and **BB2** differing only in the substitution of the 2,6-positions on the indacene framework. The synthesis of **BB1** and **BB2** starts with conversion of 4,4′-dimethyl-2,2′-bipyridine to the corresponding dicarboxylic acid (**2**) upon reaction with SeO_2 and nitric acid. Following reaction with thionyl chloride to generate the acid chloride derivative (**3**), condensation with either 2,4-dimethylpyrrole or 2,4-dimethyl-3-ethylpyrrole delivers the *bis*-dipyrromethanes that form the backbones of **BB1** and **BB2**, respectively. Reaction of the *bis*-dipyrromethanes, generated in situ, with $BF_3{\cdot}OEt_2$ and NEt_3 afforded the final bpy-BODIPY constructs. **BB1** and **BB2** were isolated in overall yields of 21% and 23%, respectively.

The structures of **BB1** and **BB2** were determined by X-ray crystallography. Single crystals of the bpy-BODIPY derivatives grew by slow evaporation of saturated chloroform or chloroform/acetonitrile solutions of the compounds. The structures (Figure 1) reveal an anti-arrangement of the BODIPY groups relative to one another. There is an inversion center in the bipyridine unit that results in a parallel arrangement of BODIPY planes within each molecule. The distances between the BODIPY moieties in each molecule are 3.4 Å for **BB1** and 3.5 Å for **BB2**, respectively. The planes of the BODIPY fragments are canted by 75° relative to the central bipyridine spacer in **BB1** and by 78° for **BB2**.

Photophysics and Electronic Structure

The basic photophysical properties of **BB1** and **BB2** were assessed in CH_2Cl_2 by a combination of UV-Vis absorption and fluorescence spectroscopy (Table 1). Both **BB1** and **BB2** display optical properties typical of BODIPY chromophores with absorption bands in the visible region centered at 504 nm and 528 nm, respectively.[49] Extinction coefficients measured for **BB1** and **BB2** are 54300 $M^{-1}cm^{-1}$ and 84100 $M^{-1}cm^{-1}$, respectively. These values are consistent with there being two BODIPY chromophores for each of the systems under consideration. Excitation into the absorption bands induces green emission for **BB1** centered at 518 nm and lower energy yellow emission for **BB2**, centered at 547 nm. The respective quantum yields for fluorescence were measured to be φ_{Fl} = 0.33 and 0.39. Absorption and emission profiles for **BB1** and **BB2** are shown in Figure 2.

Electrochemistry

Electrochemical results obtained for **BB1** and **BB2** are summarized in Table 1. Cyclic voltammetry for both BODIPY compounds in CH_2Cl_2 with 0.1 M $TBAPF_6$ reveals the accessible redox transitions. Upon reduction, **BB2** displays a single wave that is composed of two closely-spaced reduction events with voltammetric half wave potentials of −1.15 and −1.22 V vs. SCE. These potentials are slightly more positive than that of the simple alkyl substituted monomer 1,3,5,7,8-pentamethyl-2,6-ethyl-4,4-difluoro-4-bora-3a,4a-diaza-s-indacene (−1.37 V) (Figure 3a).[27,28] The oxidative wave contains two individual features at 1.11 V and 1.15 V, indicating that **BB2** is more difficult to oxidize than the corresponding BODIPY monomer (0.97 V) (Figure 3b). The high chemical reversibility of both the oxidation and reduction is consistent with the complete blocking by the 2,6-substituted ethyl groups, which prevents the subsequent decomposition of the electrochemically generated

radical cation or anion, as evidenced by the scan-rate dependences shown in Figure 3c,d. The separation of about 50 to 70 mV between two reduction and two oxidation peaks was confirmed by digital simulation (Figures 3e–l). If one assumes a simultaneous two-electron process, rather than the split wave, a significant deviation in the peak shape from the experimental results is seen (Figure 3m).

Digital simulation can be used to distinguish small separations between two oxidation and two reduction peaks. If the two BODIPY units separated by the 2,2′-bipyridine fragment interacted strongly, a considerably larger splitting would be expected. If there were no interaction, a splitting of about 36 mV (due to entropic factors) would result.[50] The observed value suggests a repulsive interaction through the bipyridine spacer, but not complete delocalization. This conclusion is consistent with the observed orthogonal orientation of the BODIPY subunits with respect to the bipyridine linker in the solid-state structures of **BB1** and **BB2** (vide supra). Moreover, DFT calculations carried out for the Bpy–BODIPY compounds indicate that both BODIPY moieties are effectively insulated from one another, with the HOMO and the LUMO for **BB1** and **BB2** residing on the individual chromophores and not delocalized onto the bipyridine spacer (Figure 4).

The reductive window of CH_2Cl_2 precludes scanning to more negative potentials beyond the first wave; however, when the solvent is changed to THF, additional reduction waves appear. These features are most likely due to irreversible reduction of the bipyridine spacer and the second reduction waves of BODIPY (Figure 3n–p). The two reduction waves of monomeric BODIPY species are split by an unusually large amount (~ 1 V), as discussed elsewhere.[30]

For **BB1** that is unsubstituted at the β-positions of the BODIPY framework, Nernstian behavior occurs upon reduction, with half wave potentials at −1.12 V and −1.17 V versus SCE (Figure 5a,b). Oxidation by CV (0.1 V/s), however, reveals two chemically irreversible half waves with potentials of 1.22 V and 1.27 V. (Figure 5a,c). These results are consistent with the electrochemistry of simple β-unsubstituted BODIPY derivatives.[28] The reduction of **BB1** to generate the radical anion (**BB1**$^{\bullet-}$) is a reversible process (Figure 5d–g), and digital simulations indicate some separation between the first and second reduction steps to generate **BB1**$^{2-}$ (Figure 5h). By contrast, the radical cation formed upon oxidation of **BB1** is unstable and susceptible to electrophilic attack.[28] This electrophilic addition shifts the observed peak potentials to less positive values, such that the thermodynamic half-wave potential for **BB1** is slightly more positive than the values reported here.

The irreversible oxidation of **BB1** is a characteristic feature of BODIPY dyes lacking alkyl or aryl substituents at the β-positions and arises from the instability of the electrogenerated radical cation toward electrophiles. While recording the oxidative scans with **BB1** we observed a dark film forming on the electrode, possibly indicating deposition of a polymeric species. This surface film increased the height of the anodic wave and to a lesser extent the corresponding cathodic wave on repeated cycling (Figure 5k). Accordingly, the electrode surface had to be repolished following oxidative scans in order to monitor consecutive studies of the solution processes. Scanning to more positive potentials showed the appearance of an additional electrochemical wave (Figure 5i,j).

In order to approximate the rate of the reaction following formation of **BB1**$^{\bullet+}$, we monitored the anodic cyclic voltammogram as a function of scan rate using MeCN as solvent. MeCN was chosen because it less resistive and amenable to faster scan rates (Figure 6). Simulations support an EEC mechanism with a pseudo first-order homogeneous rate constant of ~30 s^{-1}. There are some deviations at slower scan rates that probably originate from difficulty in

accounting for the second oxidative wave. This behavior is also evident from the slight deviation from the linear behavior observed for the scan rate dependence (Figure 6g).

Electrogenerated chemiluminescene (ECL)

ECL studies for both **BB1** and **BB2** were carried out by pulsing (1 – 30 min) to generate the radical ions and diions, but their subsequent annihilation produced only traces of light. This result can be rationalized for **BB1** in terms of the instability of the $\mathbf{BB1}^{\bullet+}$ species. The lack of an ECL response for **BB2** is less readily explained, however. Nonetheless, a strong ECL signal was obtained upon reduction of **BB2** in the presence of the co-reactant benzoyl peroxide (BPO) (Figure 7).[51–53] The ECL spectra, corresponding to yellow ECL emission for **BB2** and green ECL emission for **BB1**, are very similar to the normal fluorescence spectra when corrected for a small difference inner filter effect.[29]

$$\text{Bpy–BODIPY} + e^- \rightarrow \text{Bpy–BODIPY}^{\bullet-} \quad (1)$$

$$\text{Bpy–BODIPY}^{\bullet-} + \text{BPO} \rightarrow \text{Bpy–BODIPY} + \text{BPO}^{\bullet-} \quad (2)$$

$$\text{BPO}^{\bullet-} \rightarrow C_6H_5CO_2^- + C_6H_5CO_2^{\bullet} \quad (3)$$

$$\text{Bpy–BODIPY}^{\bullet-} + C_6H_5CO_2^{\bullet} \rightarrow \text{Bpy–BODIPY}^{*} + C_6H_5CO_2^- \quad (4)$$

$$\text{Bpy–BODIPY}^{*} \rightarrow \text{Bpy–BODIPY} + h\nu \quad (5)$$

The complete mechanism is probably more complicated than that outlined by the series of reactions above, since pulsing the potential to −1.31 V versus SCE produces the dianions. These species should also react sequentially with the BPO reactant and $C_6H_5CO_2^{\bullet}$. Moreover, comproportionation of the diradical dianions with the parent bpy-BODIPY molecule will also produce the radical anion. Another possible route involves reaction of $C_6H_5CO_2^{\bullet}$ with the parent to produce radical cation.

Summary

Two new 2,2′-bipyridine ligands containing ancillary BODIPY dyes at the 4- and 4′-positions were prepared. The basic photophysics, electrochemistry, and electrochemiluminescence of these systems have been investigated. Both **BB1** and **BB2** are strongly emissive compounds with large absorption cross sections in the visible region. Cyclic voltammetry show that the new Bpy-BODIPY ligands maintain redox properties similar to their corresponding BODIPY monomers, consistent with their solid-state structures and calculated frontier orbitals. These observations indicate that the π-system of the BODIPY chromophores is decoupled from the intervening bipyridine spacer for both systems studied. Moreover, whereas both **BB1** and **BB2** exhibit reversible reduction waves, oxidation of **BB1**, which is unsubstituted at the BODIPY β-positions, is largely irreversible. ECL studies for the Bpy-BODIPY derivatives correlate with the observed electrochemistry and both exhibit ECL spectra that are very similar to the corresponding fluorescence spectra. **BB1** displays lower intensity ECL compared to **BB2** due to competing decomposition of the reduced and oxidized intermediates through attack at the unsubstituted β-positions.

Both of the Bpy-BODIPY derivatives exhibit intense absorptions through the UV and visible regions. The ability to use these ligands with metal complexes that demonstrate

efficient charge transfer in light harvesting devices is therefore an intriguing proposal. Given that the excited state dynamics of polypyridyl complexes is intimately controlled by ligand structure[54] and that many paths can exist for electronic delocalization[55–57] and charge transfer for these systems,[58–60] many possibilities exist for the use of Bpy-BODIPY ligands in light-harvesting, energy storing and sensing applications. Accordingly, the preparation and physical interrogation of metal complexes supported by Bpy-BODIPY architectures is currently being pursued.

Supplementary Material

Refer to Web version on PubMed Central for supplementary material.

Acknowledgments

J. R. acknowledges postdoctoral fellowship support from the NIH (F32 GM080060-02). Financial support for this work (SJL) was provided by the NSF (CHE-0907905) and (AJB) Roche Diagnostics, Inc., and the Robert A. Welch Foundation (F-0021).

References

1. Blau F. Monatsh Chem. 1889; 10:375–388.
2. Katz KC, Hosseini MW. Chem Rev. 2000; 100:3553–3590. [PubMed: 11749322]
3. Kalyanasundaram, K. Photochemistry of Polypyridine and Porphyrin Complexes. Academic Press; San Diego, CA: 1992.
4. Kalyanasundaram K. Coord Chem Rev. 1982; 46:159–244.
5. Schubert US, Eschbaumer C. Angew Chem Int Ed. 2002; 41:2892–2926.
6. Balzani V, Bergamini G, Marchioni F, Ceroni P. Coord Chem Rev. 2006; 250:1254–1266.
7. Balzani V, Bergamini G, Ceroni P. Coord Chem Rev. 2008; 252:2456–2469.
8. Nazeeruddin MK, Kay A, Rodicio I, Humphry-Baker R, Mueller E, Liska P, Vlachopoulos N, Graetzel M. J Am Chem Soc. 1993; 115:6382.
9. Hagfeldt A, Boschloo G, Sun L, Kloo L, Pettersson H. Chem Rev. 2010; 110:6595–6663. [PubMed: 20831177]
10. Bignozzi CA, Argazzi R, Kleverlaan CJ. Chem Soc Rev. 2000; 29:87.
11. Geary EAM, Yellowlees LJ, Jack LA, Oswald IDH, Parsons S, Hirata N, Durrant JR, Robertson N. Inorg Chem. 2005; 44:242–250. [PubMed: 15651869]
12. Du P, Schneider J, Jarosz P, Eisenberg R. J Am Chem Soc. 2006; 128:7726–7727. [PubMed: 16771472]
13. Zhang J, Du P, Schneider J, Jarosz P, Eisenberg R. J Am Chem Soc. 2007; 129:7726–7727. [PubMed: 17547407]
14. Du P, Schneider J, Li F, Zhao W, Patel U, Castellano FN, Eisenberg R. J Am Chem Soc. 2008; 130:5056–5058. [PubMed: 18355009]
15. Owens JW, Smith R, Robinson R, Robins M. Inorg Chim Acta. 1998; 279:226–231.
16. Kadish, KM.; Smith, KM.; Guilard, R., editors. The Porphyrin Handbook. Academic Press; New York: 2000.
17. Drexhage KH. Top in App Phys. 1973; 1:155–200.
18. Lakowicz, JR. Principles of Fluorescence Spectroscopy. 3. Springer; New York: 2006. p. 67-74.
19. Adronov A, Gilat SL, Fréchet JMJ, Ohta K, Neuwahl FVR, Fleming GR. J Am Chem Soc. 2000; 122:1175–1185.
20. Lazarides T, McCormick T, Du P, Luo G, Lindley B, Eisenberg R. J Am Chem Soc. 2009; 131:9192–9194. [PubMed: 19566094]
21. Willinger K, Fischer K, Kisselev R, Thelakkat M. J Mater Chem. 2009; 19:5364–5376.
22. Dai F-R, Wu W-J, Wang Q-W, Tian H, Wong W-Y. Dalton Trans. 2011; 40:2314–2323. [PubMed: 21088788]

23. Li J-Y, Chen C-Y, Chen J-G, Tan C-J, Lee K-M, Wu S-J, Tung Y-L, Tsai J-H, Ho K-C, Wu C-G. J Mater Chem. 2010; 20:7158–7164.
24. Ziessel R, Ulrich G, Harriman A. New J Chem. 2007; 31:496–501.
25. Benniston AC, Copley G. Phys Chem Chem Phys. 2009; 11:4124–413. [PubMed: 19458813]
26. Lazarides T, McCormick TM, Wilson KC, Lee S, McCamant DW, Eisenberg R. J Am Chem Soc. 2011; 133:350–364. [PubMed: 21175161]
27. Sartin MA, Camerel F, Ziessel R, Bard AJ. J Phys Chem C. 2008; 112:10833–10841.
28. Lai RY, Bard AJ. J Phys Chem B. 2003; 107:5036–5042.
29. Nepomnyashchii AB, Bröring M, Ahrens J, Kruger R, Bard AJ. J Phys Chem C. 2010; 114:14453–14460.
30. Nepomnyashchii AB, Cho S, Rossky PJ, Bard AJ. J Am Chem Soc. 2010; 132:17550–17559.
31. Kollmannsberger M, Garries T, Heinl S, Breu J, Daub J. Angew Chem Int Ed. 1997; 36:1333–1335.
32. Trieflinger C, Röhr H, Rurack K, Daub J. Angew Chem Int Ed. 2005; 44:6943–6947.
33. Röhr H, Trieflinger C, Rurack K, Daub J. Chem Eur J. 2006; 12:689–700. [PubMed: 16231292]
34. Pangborn AB, Giardello MA, Grubbs RH, Rosen RK, Timmers FJ. Organometallics. 1996; 15:1518–1520.
35. Rosenthal J, Lippard SJ. J Am Chem Soc. 2010; 132:5536–5537. [PubMed: 20355724]
36. Bard, AJ.; Faulkner, LR. Electrochemical Methods. Fundamentals and Applications. John Wiley; New York: 1980.
37. Rudolph M. J Electroanal Chem. 1991; 314:13–22.
38. Rudolph M. J Electroanal Chem. 1992; 338:85–98.
39. Feldberg SW, Goldstein CI, Rudolph M. J Electroanal Chem. 1996; 413:25–36.
40. Mocak J, Feldberg SW. J Electroanal Chem. 1997; 378:31–37.
41. SMART. Software for the CCD Detector System. Bruker AXS; Madison, WI: 2000.
42. SAINT. Software for the CCD Detection System. Bruker AXS; Madison, WI: 2003.
43. Sheldrick, GM. SADABS: Area-Detector Absorption Correction. University of Göttingen; Göttingen, Germany: 2001.
44. Sheldrick G. Acta Crystallogr Sect A: Found Crystallogr. 2008; 64:112–122.
45. Speck, AL. PLATON, A Multipurpose Crystallographic Tool. Utrecht University; Utrecht, The Netherlands: 2001.
46. Frisch, MJ.; Trucks, GW.; Schlegel, HB.; Scuseria, GE.; Robb, MA.; Cheeseman, JR.; Montgomery, JA., Jr; Vreven, T.; Kudin, KN.; Burant, JC.; Millam, JM.; Iyengar, SS.; Tomasi, J.; Barone, V.; Mennucci, B.; Cossi, M.; Scalmani, G.; Rega, N.; Petersson, GA.; Nakatsuji, H.; Hada, M.; Ehara, M.; Toyota, K.; Fukuda, R.; Hasegawa, J.; Ishida, M.; Nakajima, T.; Honda, Y.; Kitao, O.; Nakai, H.; Klene, M.; Li, X.; Knox, JE.; Hratchian, HP.; Cross, JB.; Bakken, V.; Adamo, C.; Jaramillo, J.; Gomperts, R.; Stratmann, RE.; Yazyev, O.; Austin, AJ.; Cammi, R.; Pomelli, C.; Ochterski, JW.; Ayala, PY.; Morokuma, K.; Voth, GA.; Salvador, P.; Dannenberg, JJ.; Zakrzewski, VG.; Dapprich, S.; Daniels, AD.; Strain, MC.; Farkas, O.; Malick, DK.; Rabuck, AD.; Raghavachari, K.; Foresman, JB.; Ortiz, JV.; Cui, Q.; Baboul, AG.; Clifford, S.; Cioslowski, J.; Stefanov, BB.; Liu, G.; Liashenko, A.; Piskorz, P.; Komaromi, I.; Martin, RL.; Fox, DJ.; Keith, T.; Al-Laham, MA.; Peng, CY.; Nanayakkara, A.; Challacombe, M.; Gill, PMW.; Johnson, B.; Chen, W.; Wong, MW.; Gonzalez, C.; Pople, JA. Gaussian 03, revision D.01. Gaussian, Inc; Wallingford, CT: 2004.
47. Humphrey W, Dalke A, Schulten K. J Molec Graphics. 1996; 14:33–38.
48. Uppadine LH, Keene FR, Beer PD. J Chem Soc Dalton Trans. 2001:2188–2198.
49. Loudet A, Burgess K. Chem Rev. 2007; 107:4891–4932. [PubMed: 17924696]
50. Bard, AJ.; Faulkner, LR. Electrochemical Methods. Wiley; N.Y: 2001. p. 506
51. Chandross EA, Sonntag FI. J Am Chem Soc. 1966; 88:1089–1096.
52. Akins DL, Birke RL. Chem Phys Lett. 1974; 29:428–435.
53. Santa Cruz TD, Akins DL, Birke RL. J Am Chem Soc. 1976; 98:1677–1682.

54. Damrauer NH, Cerullo G, Yeh A, Boussie TR, Shank CV, McCusker JK. Science. 1997; 275:54–57. [PubMed: 8974388]
55. Damrauer NH, Boussie TR, Devenney M, McCusker JK. J Am Chem Soc. 1997; 119:8253–8268.
56. Damrauer NH, Weldon BT, McCusker JK. J Phys Chem A. 1998; 102:3382–3397.
57. Damrauer NH, McCusker JK. J Phys Chem A. 1999; 103:8440–8446.
58. Meylemans HA, Lei CF, Damrauer NH. Inorg Chem. 2008; 47:4060–4076. [PubMed: 18407628]
59. Meylemans HA, Damrauer NH. Inorg Chem. 2009; 48:11161–11175. [PubMed: 19856899]
60. Meylemans HA, Hewitt JT, Abdelhaq M, Damrauer NH. J Am Chem Soc. 2010; 132:11464–11466. [PubMed: 20684515]

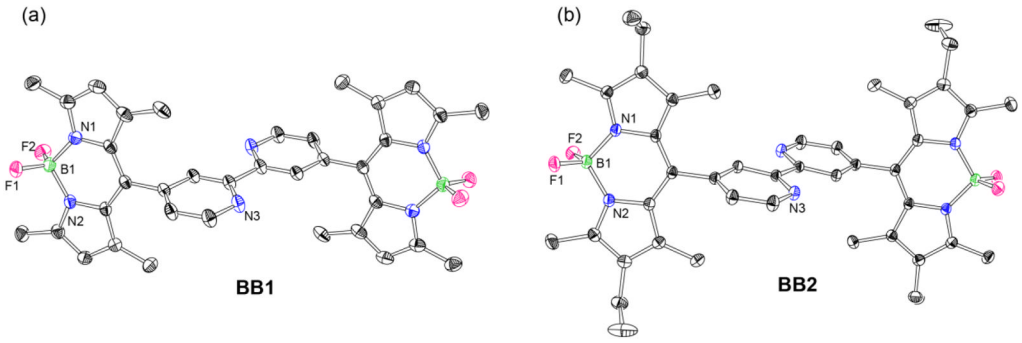

Figure 1.
Thermal ellipsoid plots for (a) **BB1** and (b) **BB2** with thermal ellipsoids shown at the 50% probability level (F Pink, B Green, C black, N blue). Hydrogen atoms are omitted for clarity.

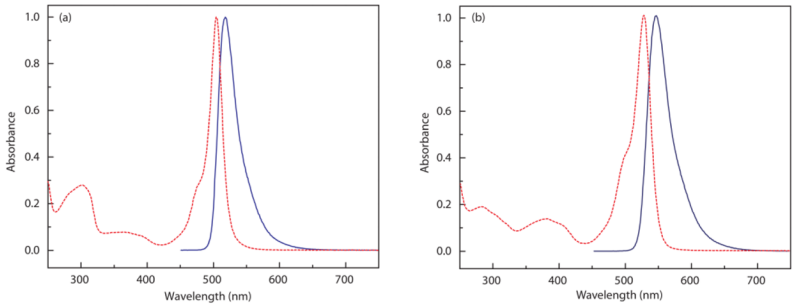

Figure 2.
Normalized absorption (---) and emission spectra (—) for (a) **BB1** and (b) **BB2**.

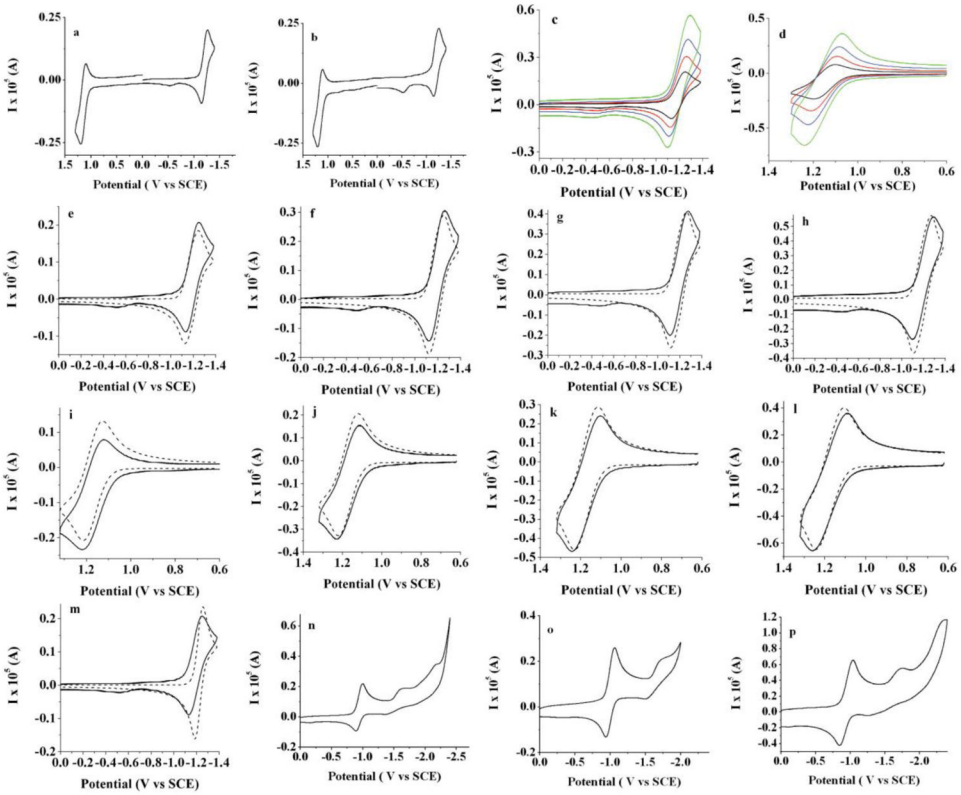

Figure 3.

Cyclic voltammograms of 0.2 mM of **BB2** (a) full scan first in the negative and (b) in the positive direction; scan rate CV dependence in (c) negative and (d) positive directions: 0.1 V/s (black line); 0.25 V/s (red line); 0.5 V/s (blue line) and 1 V/s (green line). (e)–(h) comparison of experimental results (solid line) and digital simulations (dotted line) while scanning in the negative direction and (i–l) comparison scanning in the positive direction; scan rates: (e) and (i) 0.1 V/s; (f) and (j) 0.25 V/s; (g) and (k) 0.5 V/s and (h) and (l) 1 V/s; (m) experimental data (solid line) and simulation (dotted line) at scan rate 0.1 V/s as in (e) with the simulation carried out assuming a simultaneous 2 electron reduction; (n–p) CV when scanning to more negative potentials using THF as a solvent (n,o) 0.1 V/s and (p) 1 V/s; platinum electrode area: 0.0314 cm^2, 0.1 M $TBAPF_6$ was used as a supportive electrolyte; solvent: methylene chloride except (n–p); an uncompensated resistance of 5000 Ω, capacitance of 1×10^{-7} F, α=0.5 and $k^\circ=10^4$ cm/s (chosen to show diffusion control process) was used in the digital simulations.

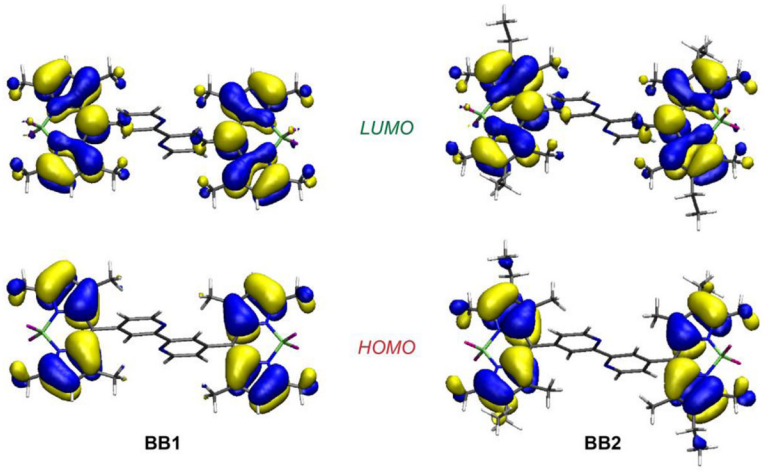

Figure 4.
Calculated frontier molecular orbitals for **BB1** and **BB2** by DFT (B3LYP/6-311G(d)).

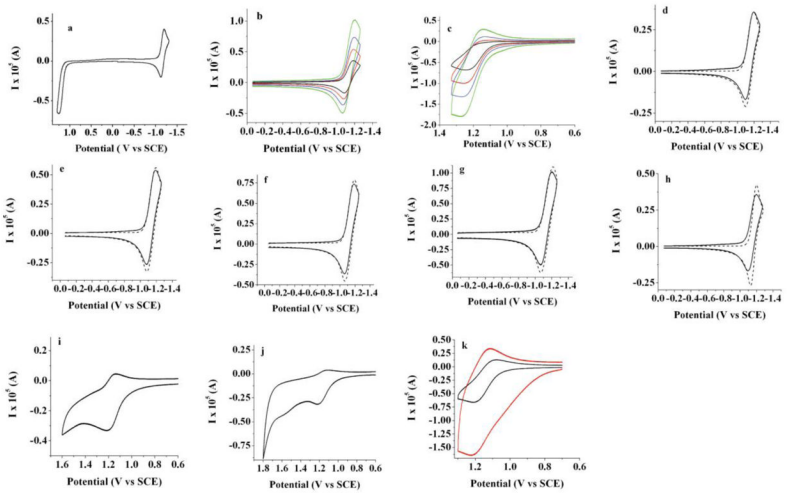

Figure 5.

Cyclic voltammograms of 0.36 mM of **BB1**: (a) full scan in the positive direction; scan rate CV dependence in (b) negative and (c) positive directions: 0.1 V/s (black line); 0.25 V/s (red line); 0.5 V/s (blue line) and 1.0 V/s (green line); comparison of experimental results (straight line) and digital simulations (dotted line) while scanning in negative direction (d–g); scan rates: (d) 0.1 V/s; (e) 0.25 V/s; (f) 0.5 V/s and (g) 1 V/s; (h) experimental data (straight line) and simulation (dotted line) at scan rate 0.1 V/s as in (d) with the simulation carried out assuming simultaneous 2 electron reduction; platinum electrode area: 0.0314 cm^2, 0.1 M $TBAPF_6$; solvent: methylene chloride; resistance: 3000 Ω, capacitance of 3×10^{-7} F, α=0.5 and $k°=10^4$ cm/s (chosen to show diffusion control process) was used for digital simulations(i) and (j) CVs at 0.1 V/s for 0.23 mM **BB1** while scanning in positive direction to 1.4 V and 1.6 V; (k) CVs at 1 V/s while scanning in positive direction during first scan (black line) and after consecutive oxidation cycles (red line) for the same concentration as (i) and (j); platinum electrode area: 0.0314 cm^2, 0.1 M $TBAPF_6$; solvent: methylene chloride; resistance: 3000 Ω, capacitance of 3×10^{-7} F, α=0.5 and $k°=10^4$ cm/s (chosen to show diffusion controlled process) was used for digital simulations.

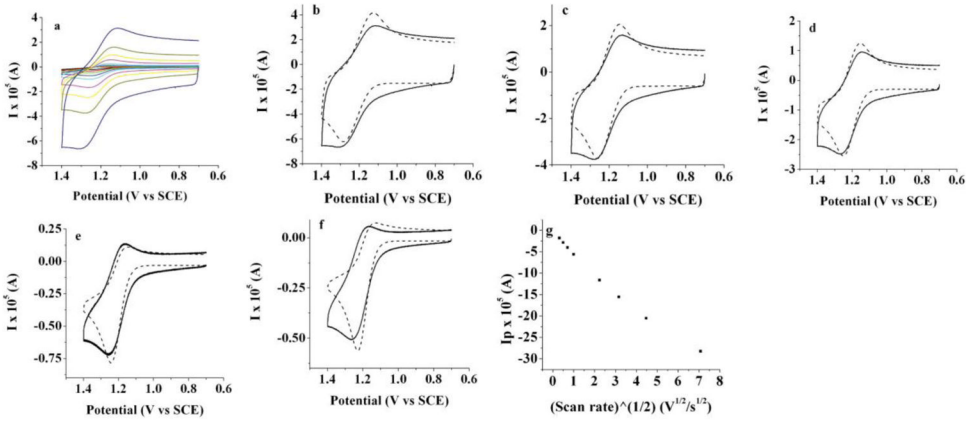

Figure 6.

Cyclic voltammetry studies of 0.23 mM **BB1** in MeCN; scan rate CV dependence in positive direction; comparison of experimental results (straight solid line) and digital simulations (dotted line) while scanning in positive direction (b–f); scan rates: (b) 50 V/s; (c) 20 V/s; (d) 10 V/s and (e) 1.0 V/s; (f) 0.5 V/s; (g) dependence of peak potential on the square root of the scan rate; platinum electrode: 0.0314 cm^2; 0.1 M $TBAPF_6$; resistance: 600 Ω, capacitance of 3×10^{-7} F, α=0.5, k°=10^4 cm/s (chosen to show diffusion controlled process) and k = 30 s^{-1} was used for digital simulations.

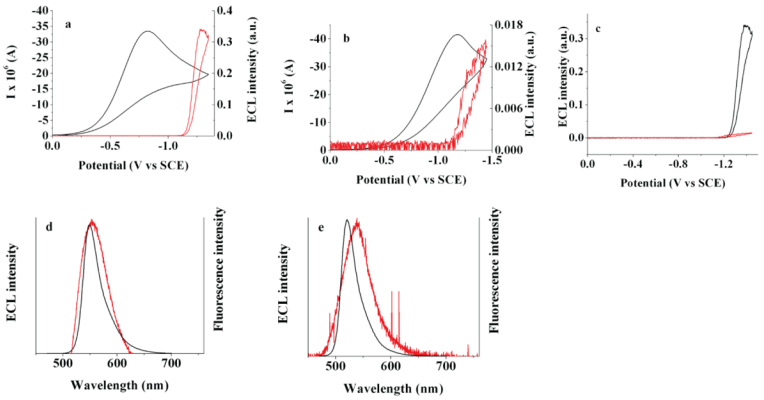

Figure 7.

(a) and (b) ECL (red line)-CV (black line) simultaneous measurements for (a) **BB2** and (b) **BB1** in the presence of 3.5 mM benzoyl peroxide for (a) and 4 mM for (b); (c) comparison of ECL signals for the case of **BB2** (black line) and **BB1** (red line); (d) and (e) ECL (red line) and fluorescence (black line) spectra for 0.2 mM of **BB2** and 0.36 mM of **BB1** in the presence of 3.5 mM of benzoyl peroxide for **BB2** and 4.0 mM for **BB1**; spectra were generated by pulsing potential from 0 V to −1.31 V versus SCE for 1 min for **BB2** and from 0 V to −1.27 V for **BB1**; platinum electrode area: 0.0314 cm^2 in CH_2Cl_2/0.1 M $TBAPF_6$.

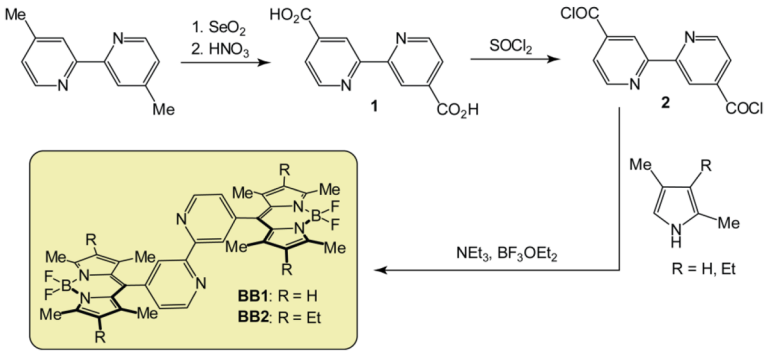

Scheme 1.
Synthesis of **BB1** and **BB2.**

Table 1

Photophysical and electrochemical data for **BB1** and **BB2**. All potentials reported vs SCE.

	Photophysics		*Electrochemistry*			
Compound	**Abs (λ_{max})**	**Em (λ_{max})**	**$E_{1/2}(A/A^{+})$**	**$E_{1/2}(A/A^{-})$**	**ECL (λ_{max})**	**$D \cdot 10^{6}$**
BB1	504 nm	518 nm	1.22, 1.27	−1.12, −1.17	533 nm	4.0 (cm^2/s)
BB2	528 nm	547 nm	1.11, 1.15	−1.15, −1.22	554 nm	4.0 (cm^2/s)